Journal of Solid State Chemistry 183 (2010) 3052–3057

Contents lists available at ScienceDirect

Journal of Solid State Chemistry

journal homepage: www.elsevier.com/locate/jssc

Origin of the improved photo-catalytic activity of F-doped $ZnWO_4$: A quantum mechanical study

Honggang Sun [a], Weiliu Fan [b,*], Yanlu Li [a], Xiufeng Cheng [a], Pan Li [a], Xian Zhao [a,*]

[a] State Key Laboratory of Crystal Materials, Shandong University, Jinan 250100, China
[b] Department of Chemistry and Chemical Engineering, Shandong University, Jinan 250100, China

ARTICLE INFO

Article history:
Received 29 March 2010
Received in revised form
8 October 2010
Accepted 16 October 2010
Available online 30 October 2010

Keywords:
F-doping
$ZnWO_4$
Photo-catalysis
DFT
Reduced center
Red shift

ABSTRACT

Two different mechanisms for improving photo-catalytic activity in different types of F-doped $ZnWO_4$ are tentatively proposed, based on density function theory calculations. When the lattice O atom is substituted by one F atom, our calculations show that a reduced W^{5+} center adjacent to the doped F atom will act as a trap for the photo-induced electron, and will thus result in a reduction of electron–hole recombination and improvement of the photo-catalytic activity. For the interstitial F-doped model, partial F 2*p* states mixing with O 2*p* states localize above the top of the valence band and act as the frontier orbital level. Electronic transitions from these localized states induce a red shift of about 54 nm of the optical absorption edge. This work shows that F-doped $ZnWO_4$ will be a promising photo-catalyst with favorable photo-catalytic activity in the UV region.

1. Introduction

An increased awareness of environmental and energy issues has led to a new focus on the development of clean and renewable energy sources. Since Fujishima and Honda [1] demonstrated that crystalline TiO_2 could split water, producing H_2 and O_2 after photoexcitation, the application of wide band gap semiconductor oxides on photo-catalytic technology has led to worldwide attention in finding solutions to these issues. However, in most stable semiconductor photo-catalysts, the overall efficiency is still too low and greatly restricts their commercial use due to their narrow light-response range and low probability of separation of the photo-induced electron–hole pairs. To solve these issues, numerous studies in the past three decades have been conducted involving crystal growth, doping and hetero-structural design of high-efficiency semiconductor photo-catalysts. Thus far, the introduction of various impurities into the semiconductor host has caused worldwide interest and shown to produce better photo-catalytic activity, widely known as energy band engineering. Initially, researchers introduced transition metals (TM) into the semiconductors to get a visible light response [2–8]. However, TM materials have some disadvantages for efficient water splitting reactions, such as poor photocurrent density due to rapid electron–hole recombination and thermal instability. To solve these problems, nonmetal doping has been considered, and has shown some promising results [9–22].

It has been confirmed that tungstate materials, such as Bi_2WO_6 [23] and $AgInW_2O_8$ [24], show high photo-catalytic activity on decontamination. One of the tungstate family, $ZnWO_4$, has been used for water splitting and mineralization of organic pollutants under UV irradiation [25–27]. However, its industrial application is hampered because the photo-catalytic activity of $ZnWO_4$ is not high enough for practical applications. To solve this disadvantage, fluorine anions have been introduced to the substrate by Zhu et al. [28,29]. Their experiments have shown promising photo-catalytic activity for F–$ZnWO_4$ with UV radiation. As we know, the chemical nature and lattice location of the introduced species are two important issues playing a crucial role in determining the photo-catalytic activity.

In the previous work, we have also achieved better photo-catalytic activity in the interstitial F-doped $ZnWO_4$ nanostructure [30]. The photoelectrochemical analysis indicated that the interstitial fluorine doping promotes the transfer of the photogenerated electrons from the inner regions to the surface and the photocurrent density was about 5 times than that of undoped $ZnWO_4$. And under UV light illumination, a rapid decrease of RhB absorption at a wavelength of 553 nm was observed from photo-catalytic experiments for the interstitial F-doped $ZnWO_4$. In further research, we found a different photo-catalytic mechanism in the F substituted O-doped $ZnWO_4$, which also shows promising photo-catalytic activity.

In the present paper, to obtain microscopic insight into the different effects of F-doping on improving the photo-catalytic

* Corresponding authors. Fax: +86 531 88364864.
E-mail addresses: fwl@sdu.edu.cn (W. Fan), zhaoxian@icm.sdu.edu.cn (X. Zhao).

0022-4596/$ - see front matter © 2010 Elsevier Inc. All rights reserved.
doi:10.1016/j.jssc.2010.10.021

activity of $ZnWO_4$, we have constructed appropriate F substituted and interstitial doped $ZnWO_4$ configurations and carried out an accurate comparative analysis of the geometric and electronic structures for pure and doped models using DFT calculations. The results provide a solid basis for the different rationalization of experimentally observed improvements in the photo-activity as a consequence of the different F-doping species.

2. Computational details and structural aspects

The calculations are performed using spin-polarized density function theory (DFT) using the Cambridge Sequential Total Energy Package (CASTEP) [31]. The PBE function in the generalized gradient approximation (GGA) [32] is treated with the exchange correlation potential. Ultrasoft pseudopotentials are used to deal with core electrons. In the PBE calculations, a plane wave basis set is used. The cutoff energy for the smooth part of the wave function is 340 eV. Following published data [28–30], monoclinic $ZnWO_4$ has been used in our calculations. For the pure $ZnWO_4$ cell, when the calculations of the geometry optimization are carried out, the k space integrations are carried out with the Monkhorst-Pack grid [33] using $5\times4\times5$ k-points. The self-consistent convergence accuracy is set at 1×10^{-5} eV/atom, the convergence criterion for the force between atoms is 3×10^{-2} eV/Å and the maximum displacement is 1×10^{-3} Å. The crystal parameters of the optimized structure are listed in Table 1, and are very consistent with experiments [34].

To study F-doped configurations in this work, we consider a $2\times2\times2$ (96-atom) $ZnWO_4$ supercell based on the optimized cell. Two ways are used to introduce one F atom into the lattice of the $ZnWO_4$ supercell. The first is to replace a lattice oxygen atom with a fluorine atom, giving the substitutional configuration, which is labeled F_s. In the $ZnWO_4$ crystal, there are two different O atoms (as seen in Table 1), O1 is bonded to two W atoms and one Zn atom, and O2 is bonded to two Zn atoms and one W atom. Therefore, two different substitutional sites are considered, and the structures and energies of the two optimized supercells are shown in the Supplementary Data (S1). Our calculations indicate that the electronic structures of the two models are similar, so only the most stable structure (F- to O1-site) is discussed in this paper. Another doping condition is that a fluorine atom is positioned at an interstitial site, giving the interstitial configuration, represented as F_i. Several different interstitial sites are also taken into account and some optimized structures are shown in supplementary information S2. Likewise only the structure of lowest energy is considered in the present discussion. For all supercell structures, full geometry optimization is performed at the Γ point and an accurate density of the electronic states is achieved with $3\times2\times3$ k-points. All the electronic structures are calculated for the corresponding optimized crystal geometries.

The absorption spectra can be obtained from the real and imaginary part of the dielectric constant obtained from the DFT calculations. The imaginary part of the dielectric constant ε_2 is described as

$$\varepsilon_2(\omega)=\frac{2\pi^2e^2}{\Omega\varepsilon_0}\sum_{i\in c,f\in v}\sum_k|\langle\Psi_k^c|\hat{\mu}\cdot r|\Psi_k^v\rangle|^2\delta[E_k^c-E_k^v-\hbar\omega],$$

where Ω is the volume of the elementary cell, k represents the k point,ω the frequency of the incident light, and c and v represent the conduction and valence bands, respectively. Ψ_k^c and Ψ_k^v are the eigenstates, r the momentum operator, and $\hat{\mu}$ the external field vector.

The real part of the dielectric constant ε_1 can be derived from ε_2 using the Kramers–Kronig relations [35]

$$\varepsilon_1(\omega)=1+\left(\frac{2}{\pi}\right)\int_0^\infty d\omega'\frac{\omega'^2\varepsilon_2(\omega')}{\omega'^2-\omega^2}.$$

The absorption coefficient α (ω) can be derived from the following formula [36,37]:

$$\alpha(\omega)=\sqrt{2}\omega\left[\sqrt{\varepsilon_1^2(\omega)+\varepsilon_2^2(\omega)}-\varepsilon_1(\omega)\right]^{1/2}.$$

3. Results and discussions

3.1. Geometrical structures

Fig. 1 gives the optimized structures of pure and F-doped $ZnWO_4$ used in the present work. For the F_s-doped structure (Fig. 1b), the whole structural variations following O replacement with F are found to be slight after geometry optimization. The F–Zn bond is stretched from 2.075 to 2.239 Å with respect to the corresponding O–Zn bond in pure $ZnWO_4$. Also, the two F–W bonds are stretched to 2.065 and 2.269 Å compared with the original O–W bonds 1.919 and 2.158 Å. For the interstitial model of lowest energy (Fig. 1c), the fluorine atom is bound to two lattice W atoms and the resulting F–W bonds are 2.212 and 2.251 Å, respectively. The distances between the F impurity and the nearest O atoms are about 2.036 Å, which suggests that there may be interactions between F and O atoms in the lattice.

To understand the charge redistribution induced by different types of fluorine impurity, we calculate the electron density and different density maps of the two F-doped $ZnWO_4$ supercells which are shown in Fig. 2. The Mulliken population analyzes for charge are also calculated and listed in Table 2. In the substitutional F- to O-doped model (Fig. 2a and a′), the bonds F–W and F–Zn are predominantly ionic bonds characteristically formed by capturing electrons from adjacent W and Zn. The calculated charge on the F anion is about $-0.48e$, which is less than the original O ion ($-0.70e$). For the cations bonded to the F anion, the charge on the Zn ion is about $1.25e$, unchanged compared with the pure phase, while two adjacent W ions have decreased their charge to 1.30 and $1.40e$ (originally W $1.44e$). These results indicate that the insertion of the F^- ion in the O^{2-} sites of the $ZnWO_4$ lattice induces one extra electron for charge compensation. And thus the interaction between F anion and W cations is getting weak and the F–W bonds are longer than original O–W bonds.

Table 1
The structural parameters of pure monoclinic $ZnWO_4$ obtained by GGA calculations.

Compound space group	Unit cell (Å)	Atom	Wyckoff site	x	y	z
Monoclinic $ZnWO_4$ $P2/C$	a=4.751 (4.720)[a]	W	2e	0.000 (0.000)[a]	0.180 (0.179)[a]	0.250 (0.250)[a]
	b=5.840 (5.700)[a]	Zn	2f	0.500 (0.500)[a]	0.681 (0.674)[a]	0.250 (0.250)[a]
	c=4.972 (4.950)[a]	O1	4g	0.214 (0.220)[a]	0.106 (0.110)[a]	0.937 (0.950)[a]
	V=137.952 (133.175)[a]	O2	4g	0.255 (0.260)[a]	0.371 (0.380)[a]	0.402 (0.390)[a]

[a] See Ref. [31].

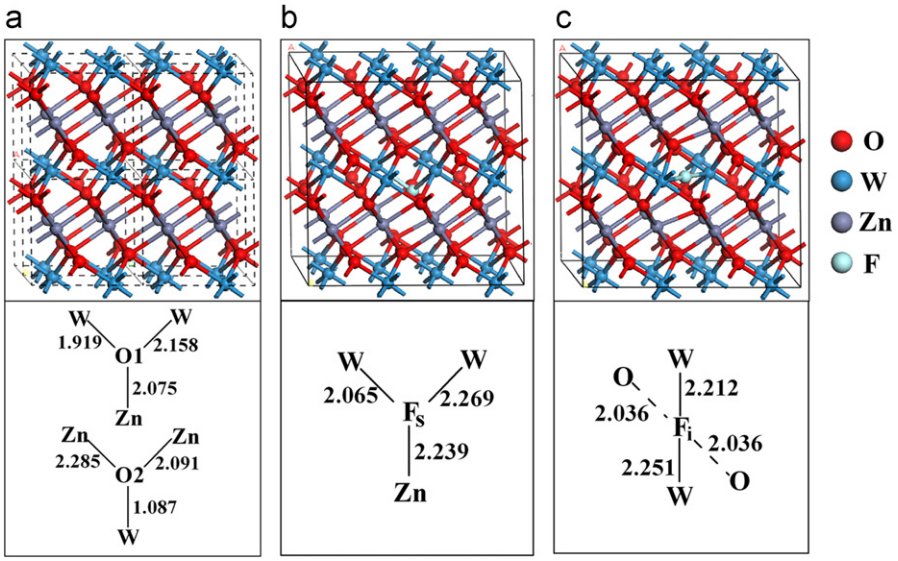

Fig. 1. The structures of (a) pure phase, (b) F_s-doped supercell and (c) F_i-doped supercell. And the partial structures are also shown.

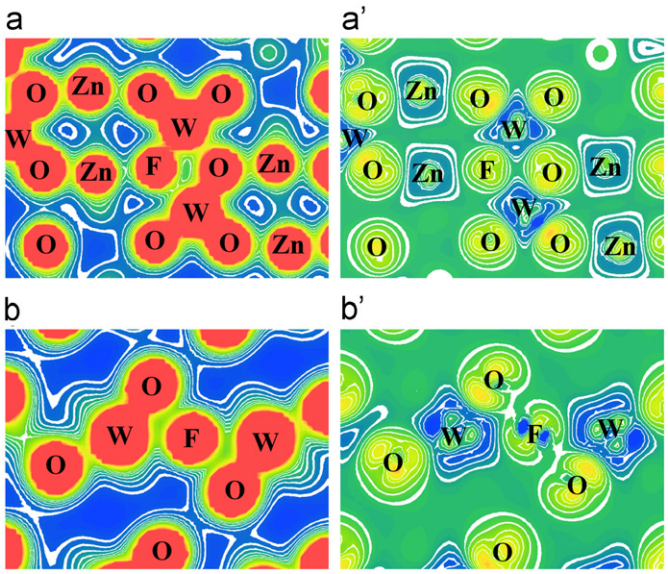

Fig. 2. Total electron density maps (left) and electrons difference density maps (right) for (a), (a′) F_s-doped supercell and (b), (b′) F_i-doped supercell.

Table 2
The Mulliken population on the F atom, two W atoms bonded to a F atom in F_s- and F_i-doping, the original O atom substituted by a F atom, and the nearest two O atoms in the F_i-doped model.

Model	Charge population			
	W	Zn	O	F
Pure phase	1.44	1.25	−0.70, −0.65	
F_s	1.30, 1.40	1.25	−0.70	−0.48
F_i	1.46, 1.47	1.25	−0.55, −0.55	−0.38

The extra electron is localized on the adjacent W cation, causing its reduction from W^{6+} to W^{5+}. To give detailed information of this process, a more accurate analysis has been performed for the spin properties by a doublet ground state calculation. As shown in Fig. 3a,

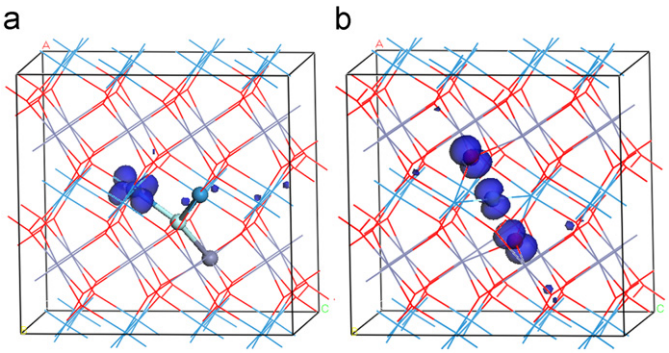

Fig. 3. The spin density maps of (a) F_s-doped supercell and (b) F_i-doped supercell.

the excess electron introduced by F is distributed over the W ions in the supercell and localized on a W d_{xz} state. We denote this process using the simple formula $[WO_4]^{2-}+xF \rightarrow W_x^{5+}W_{1-x}^{6+}O_{4-x}^{2-}F_x+(x/2)O_2$. The reduced W^{5+} center in the lattice is also confirmed in the next discussion concerning the electronic structure.

As shown in Fig. 2b and b′, in the F_i-doped model, two predominantly ionic F–W bonds are formed through the electrons transfer from adjacent W ions to F ion. The charge on the F ion is $-0.38e$ and is captured from the two bonding W ions (1.46 and 1.47e). The two adjacent O ions show a charge decrease to $-0.55e$ compared with the original $-0.65e$. The calculation reveals that some of the charges on the F ions have been obtained from the adjacent O ions. These bonding properties are different to the interstitial N-doping semiconductors, which produce a NO_x species in the lattice [14]. We attribute the difference to the stronger electronegativity of the F atom compared with oxygen, which indicates a negative fluorine oxidation state will preferably be formed in the structure. Due to the single electron on the F impurity, a spin density analysis was also carried out. Fig. 3b shows that the spin density is not only localized on the F atom but also around the two adjacent O atoms displaying a 2p characteristic. This result indicates that a coupling spin may exist between the F impurity and the lattice O, which will induce a change of electronic structure and influence the photo-catalytic process. A more detailed discussion is given in the next section.

3.2. Electronic structures

To study the changes of band structures in F-doped $ZnWO_4$, spin polarized calculations have been performed and the calculated results are plotted in Fig. 4. Insight into the bonding interaction between the F-dopant and the original constituents can be obtained from the total density of states (DOS) shown in Fig. 5A. Moreover, analysis of the projected density of states (PDOS) in Fig. 5B gives detailed information about the origin of the changes of electronic energy levels for F-doped $ZnWO_4$.

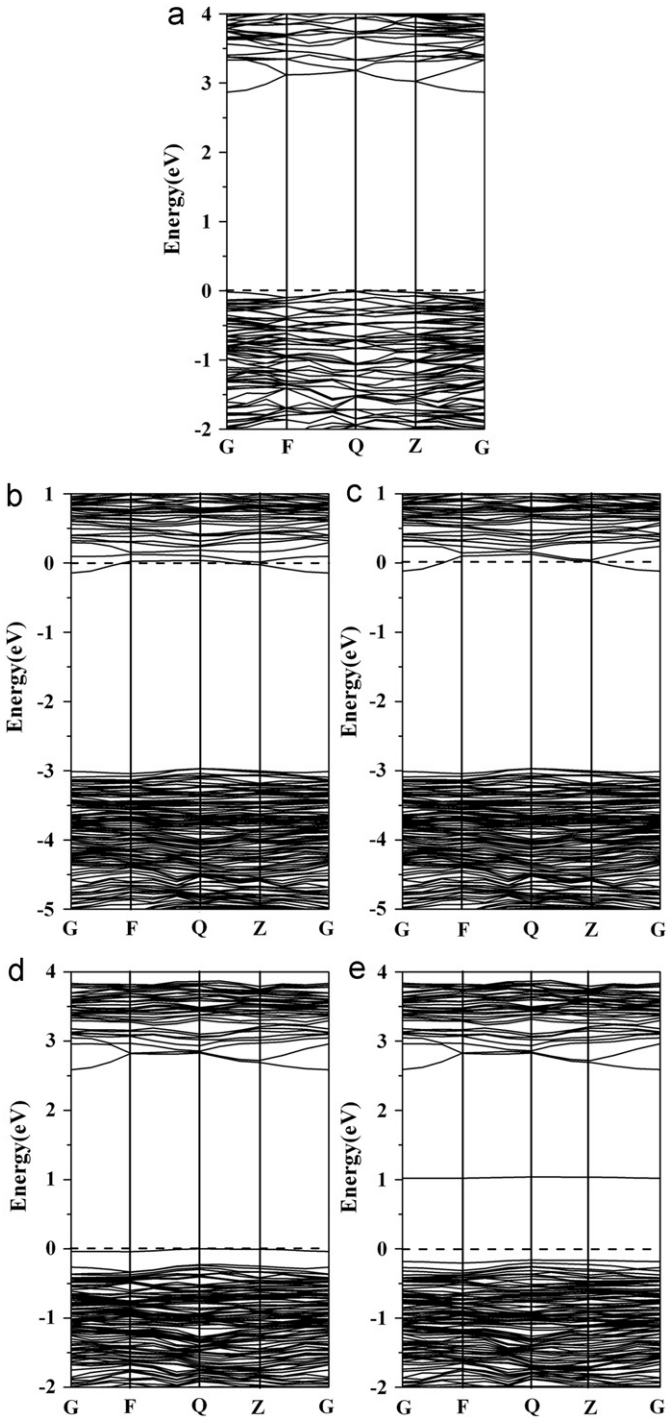

Fig. 4. The band structures of (a) pure phase, (b, c) spin up and down channels of F_s-doped supercell, and (d, e) spin up and down channels of F_i-doped supercell. The dash lines represent the Fermi level.

The calculated band gap in Fig. 4a is about 2.88 eV, which is smaller than the experimental value of about 3.69 eV [26]. The band gap underestimation from DFT always exists due to the well-known limitation of predicting accurate conduction band properties [38]. However, it is still a widely accepted method for discussion of the properties of the valence band, and this gives reasonable explanation for the experimental results because only the relative positions of the occupied states and empty states need be taken into account. As shown in Fig. 5a and a′, the main contribution to the topmost valence band (VB) of pure $ZnWO_4$ is from the O 2*p* states, which have noticeable hybridization interaction with the Zn 3*d* and minor W 5*d* states below −3 eV. Also, the bottommost conduction bands (CBs) mainly originate from the W 5*d* states and have little O 2*p* contribution. These results indicate that the electronic *p*–*d* interband excitation between O and W is responsible for the optical absorption edge.

For the F_s-doped $ZnWO_4$, Fig. 4b and c gives the up and down spin band channels, respectively. In the present calculations, no band gap narrowing is predicted. However, compared with the pure phase, some energy levels at the bottom of the CB are more dispersive. As is known, if the band is very dispersive, recombination of the electrons and holes through this band is not expected to be very high, which can be useful for the photoexcitation of electrons from the VB to the CB in the photo-catalytic process. The calculated DOS in Fig. 5b shows that the VB maximum has a larger moving to the lower energy. The Fermi level is pinned in the bottom of the CB, indicating that some donor levels are formed due to the F_s-doping. The further PDOS (Fig. 5b′) show that most of the F 2*p* states are localized at lower energies (mixing with the VB states) and no F 2*p* states are in the gap. This result is different to the calculations of the substitutional nitrogen doping in semiconductor oxides which give a gap for N 2*p* states above the top of valence band and thus induce a red shift of the optical absorption. The difference may be due to the electronegativity of F dopant is higher than that of N and O, and has the lowest *p* orbital energy [39]. The PDOS analysis for the W ions adjacent to the F-doping gives an imbalance of 5*d* states in the two spin channels in the bottom of the CB. And some occupied W 5*d* states lie below the Fermi level as a $5d^1$ state, which induces the excitation energy has a slight blue shift of about 0.10 eV due to the well-known Burstein-Moss shift of n-type doping [40]. The calculated results once again prove that reduced W^{5+} exists in the lattice. The effect of reduced W^{5+} center on the photo-catalytic activity of $ZnWO_4$ is similar to the effect of Ti^{3+} in the reduced TiO_2 [41–44]. In the photo-catalytic process, the reduced W^{5+} center favors the activation of electrons in the conduction band, their diffusion on the surface, as well as a longer e–h recombination time, thus accounting for the superior photo-catalytic activity. A detailed illustration of the mechanism that improves the photo-catalysis is plotted in Fig. 6a, which shows that the reduced W^{5+} also plays the role of transferring electrons to the surface absorptive O_2 to form a superoxide anion O_2^- described by $W^{5+}+O_2 \rightarrow W^{6+}+O_2^-$. In addition, the relatively low energy of the VB maximum compared with the Fermi level indicates a stronger oxidative ability involving the oxidation of H_2O and the degradation of the substrate on the surface; this can be described by $H_2O(sub)+h^+ \rightarrow *OH+H^+(sub)$.

For the band structures of F_i-doped $ZnWO_4$, as shown in Fig. 4d and e, one isolated level is localized at 0.25 eV above the VB for the spin up channel and 1.20 eV for the spin down channel, respectively. The analysis of the DOS and PDOS in Fig. 5c and c′ can give more information about the electronic changes. As shown in Fig. 5c, compared with the pure phase, the excitation energy from the occupied states to the CBM decreases slightly by about 0.30 eV, corresponding to the ~54 nm red shift of the optical absorption, which is agreement with our original experimental observations. For the PDOS in Fig. 5c′, the isolated level above the valence band in

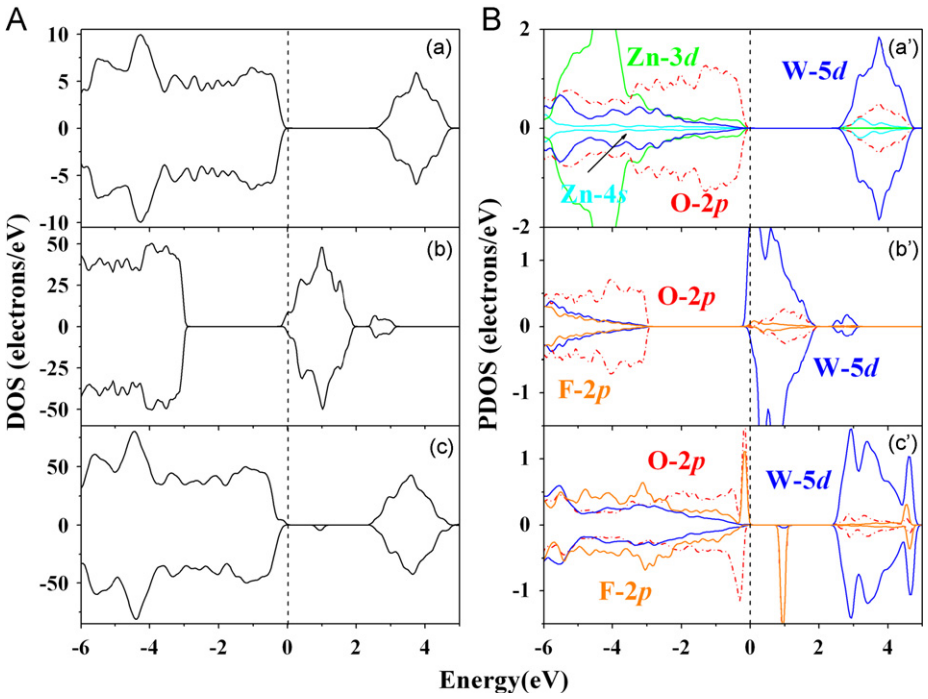

Fig. 5. (A) Total density of states (DOS) and (B) projected density of states (PDOS) for (a, a′) pure phase, (b, b′) F_s-doped supercell and (c, c′) F_i-doped supercell. The dash lines represent the Fermi level.

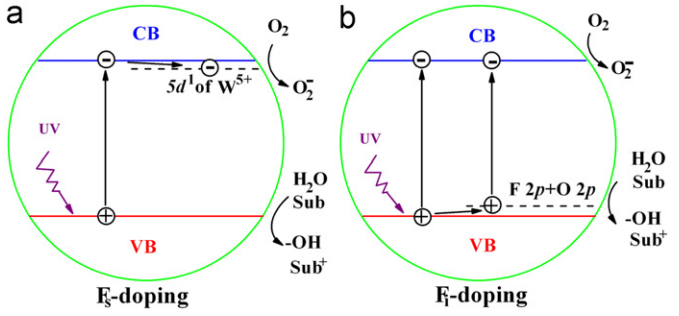

Fig. 6. The mechanisms of improving photo-catalytic activity in F-doped $ZnWO_4$, (a) F_s, and (b) F_i.

the spin up channel is mainly contributed to the mixing of F 2*p* and O 2*p* states. Therefore, the slight red shift of the excitation energy are mainly due to the mixing of states from the spin up F 2*p* and O 2*p*, which extend the bandwidth of the valence band by raising the upper level. The isolated spin down energy level localized in the gap above the Fermi level is mostly originate from the mixing of the F 2*p* and O 2*p* states, showing an unoccupied characteristic. Combined with the spin density analysis in the section above, we conclude that the gap states are present as a half-filled level which indicates that the interstitial F impurity may act as *p*-type doping, and thus supply holes as carriers to improve the photocurrent density of doped $ZnWO_4$ under UV radiation. A schematic diagram of the mechanism of improvement of the photo-catalytic activity for the F_i-doped $ZnWO_4$ is shown in Fig. 6b.

3.3. *Absorption spectra*

We have also calculated and illustrated the variation of the optical absorption spectra for the fluorine doped $ZnWO_4$. For a comparison with the experimentally observed band gap of pure $ZnWO_4$ polymorphs, which is 3.69 eV, a scissor of 0.80 eV has been used in our analysis. As shown in Fig. 7, the knee at about 320 nm

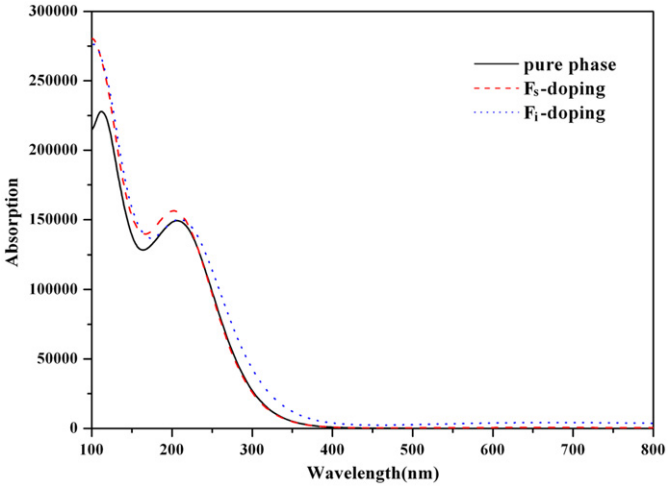

Fig. 7. The calculated absorption spectra for pure and F-doped $ZnWO_4$.

for pure $ZnWO_4$ corresponds to its band gap energy. In the F_s-doped model, the calculated optical absorption edge shows no change compared to the pure phase, which is in agreement with the discussion of the band structure. This phenomenon indicates that the enhancement of photo-catalytic activity is not due to the improvement of the optical absorption but instead the formation of reduced W^{5+} centers. In the F_i-doped model, the edge of the optical absorption is at about 370 nm showing a slight red shift of about 50 nm, which has been attributed to the electronic excitation from the mixing of the F 2*p* and O 2*p* states above the VB.

4. Conclusions

On the basis of the calculated results, two different electronic transition mechanisms are proposed to explain the improvement of the UV light photo-activity by F substitutional and interstitial

doped $ZnWO_4$. When F substitutes for O in the lattice, our results indicate that a reduced $5d^1$ state, originating from the W^{5+}, will act as a trap for the photo-induced electron, and thus result in a reduction of the electron–hole recombination and the improvement of photo-catalytic activity. When F is located at the interstitial positions, our calculations note a partial mix of N 2*p* states with O 2*p* states localized above the top of the valence band, acting as the frontier orbital level. Electronic transitions from these localized states induce a slight ~0.30 eV red shift of the optical absorption edge. We also note that interstitial F-doping induces an empty state above the VBM to supply hole carriers and thus improve the photocurrent density. This is very good for improving the photocurrent density and enhancing the catalytic efficiency of photo-catalytic reactions.

Supplementary information available

Several optimized geometry structures of F_s- and F_i-doped $ZnWO_4$ are shown in the supplementary information. This material is available free of charge via the Internet at http://www.sciencedirect.com.

Acknowledgments

This work is supported by the National Natural Science Foundation of China (Grant nos. 50802056 and 50721002), 973 Program of China under Grant no. 2009CB930103, Youth Scientist (Doctoral) Foundation of Shandong Province of China under Grant no. BS2009CL038, Specialized Research Fund for the Doctoral Program of Higher Education of China under Grant no. 20070422060, and the Independent Innovation Foundation of Shandong University (IIFSDU) under Grant no. 2009TS016.

Appendix A. Supplementary material

Supplementary data associated with this article can be found in the online version at doi:10.1016/j.jssc.2010.10.021.

References

[1] A Fujshima, K Honda, Nature 238 (1972) 37.
[2] S. Klosek, D. Raftery, J. Phys. Chem. B 105 (2001) 2815.
[3] A. Di Paola, G. Marci, L. Palmisano, M. Schiavello, K. Uosaki, S. Ikeda, B. Ohtani, J. Phys. Chem. B 106 (2002) 637.
[4] J.J. Sene, W.A. Zeltner, M.A. Anderson, J. Phys. Chem. B 107 (2003) 1597.
[5] E.P. Reddy, B. Sun, P.G. Smirniotis, J. Phys. Chem. B 108 (2004) 17198.
[6] A.K Ghosh, H.P. Maruska, J. Electrochem. Soc. 124 (1977) 1516.
[7] E. Borgarello, J. Kiwi, M. Gra zel, E. Pelizzetti, M. Visca, J. Am. Chem. Soc. 104 (1982) 2996.
[8] G. Shao, J. Phys. Chem. C 112 (2008) 18677.
[9] S.U.M. Khan, M. Al-Shahry, W.B. Ingler Jr., Science 297 (2002) 2243.
[10] H. Luo, T. Takata, Y. Lee, J. Zhao, K. Domen, J. Zhao, Y. Yan, Chem. Mater. 16 (2004) 846.
[11] B. Neumann, P. Bogdanoff, H. Tributsch, S. Sakthivel, H. Kisch, J. Phys. Chem. B 109 (2005) 16579.
[12] J.H. Park, S. Kim, A.J. Bard, Nano Lett. 6 (2006) 24.
[13] W.Y. Su, Y.F. Zhang, Z.H. Li, L. Wu, X.X. Wang, J.Q. Li, X.Z. Fu, Langmuir 24 (2008) 3422.
[14] (a) C. Di Valentin, G. Pacchioni, A. Sellonoi, Phys. Rev. B 70 (2004) 085116;
(b) C. Di Valentin, G. Pacchioni, A. Sellonoi, S. Livraghi, E. Giamello, J. Phys. Chem. B 109 (2005) 11414;
(c) C. Di Valentin, G. Pacchioni, A. Sellonoi, S. Livraghi, Chem. Mater. 17 (2005) 6656;
(d) S. Livraghi, M.C. Paganini, E. Giamello, A. Selloni, C. Di Valentin, G. Pacchioni, J. Am. Chem. Soc 128 (2006) 15666;
(e) A.M. Czoska, S. Livraghi, M. Chisea, E. Giamello, S. Agnoli, G. Granozzi, E. Finazzi, C. Di Valentin, G. Pacchioni, J. Phys. Chem. C 112 (2008) 8951.
[15] R. Asahi, T Morikawa, T. Ohwaki, K. Aoki, Y. Taga, Science 293 (2001) 269.
[16] H. Irie, Y. Watanabe, K. Hashimoto, J. Phys. Chem. B 107 (2003) 5483.
[17] (a) O. Diwald, T.L. Thompson, E.G. Goralski, S.D. Walck, J.T. Yates Jr, J. Phys. Chem. B 108 (2004) 52;
(b) O. Diwald, T.L. Thompson, T. Zubkov, E.G. Goralski, S.D. Walck, J.T. Yates Jr, J. Phys. Chem. B 108 (2004) 6004.
[18] X. Chen, C. Burda, J. Phys. Chem. B 108 (2004) 15446.
[19] M. Miyauchi, A. Ikezawa, H. Tobimatsu, H. Irie, K. Hashimoto, Phys. Chem. Chem. Phys. 6 (2004) 865.
[20] T. Sano, N. Negishi, K. Koike, K. Takeuchi, S. Matsuzawa, J. Mater. Chem. 14 (2004) 380.
[21] (a) E.A. Reyes-Gacria, Y.P. Sun, D. Raftery, J. Phys. Chem. C 111 (2007) 17146;
(b) E.A. Reyes-Gacria, Y.P. Sun, D. Raftery, J. Electrochem. Soc. 153 (2006) A1296.
[22] M. Mrowetz, E. Selli, Phys. Chem. Chem. Phys. 7 (2005) 1100.
[23] J.W Tang, Z.G. Zou, J.H. Ye, Catal. Lett. 92 (2004) 53.
[24] J.W. Tang, Z.G. Zou, J.H. Ye, J. Phys. Chem. B 107 (2003) 14265.
[25] X. Zhao, Y.F. Zhu, Environ. Sci. Technol. 40 (2006) 3367.
[26] J. Lin, J. Lin, Y.F. Zhu, Inorg. Chem. 46 (2007) 8372.
[27] S. Lin, J.B. Chen, X.L. Wen, L.Y Yang, X.Q. Chen, Mater. Res. Bull. 44 (2009) 1102.
[28] G.L. Huang, Y.F. Zhu, J. Phys. Chem. C 111 (2007) 11952.
[29] G.L. Huang, S.C. Zhang, T.G. Xu, Y.F. Zhu, Environ. Sci. Technol. 42 (2008) 8516.
[30] S.H. Chen, H.G. Sun, W.L. Fan, X. Zhao, X. Sun, S.X. Sun, J. Phys. Chem. C 114 (2010) 7680.
[31] M.D. Segall, P.J.D. Lindan, M.J. Probert, C.J. Pickard, P.J. Hasnip, S.J. Clark, M.C. Payne, J. Phys.: Condens. Matter 14 (2002) 2717.
[32] J.P. Perdew, K. Burke, M. Ernzerhof, Phys. Rev. Lett. 77 (1996) 3865.
[33] H.J Monkhorst, J.D. Pack, Phys. Rev. B 13 (1976) 5188.
[34] O.S. Filipenko, E.A. Pobedimskaya, N.V. Belov, Kristallografiya 13 (1968) 163.
[35] P.Y. Yu, M. Cardona, Fundamentals of Semiconductors, Springer-Verlag, Berlin, 1996.
[36] S. Saha, T.P. Sinha, Phys. Rev. B 62 (2000) 8828.
[37] M.Q. Cai, Z. Yin, M.S. Zhang, Appl. Phys. Lett. 83 (2003) 2805.
[38] R.M. Martin, Electronic Structure: Basic Theory and Practical Methods, Cambridge University Press, Cambridge, England, 2004.
[39] J.B. Li, S.-H. Wei, S.-S Li, J.-B. Xia, Phys. Rev. B 74 (2006) 081201.
[40] E. Burstein, Phys. Rev. 93 (1954) 632.
[41] G. Mattioli, F. Filippone, P. Alippi, A.A. Bonapasta1, Phys. Rev. B 78 (2008) 241201.
[42] N.A. Deskins, R. Rousseau, M. Dupuis, J. Phys. Chem. C 114 (2010) 5891.
[43] J.D. Zhuang, W.X. Dai, Q.F. Tian, Z.H. Li, L.Y. Xie, J.X. Wang, P. Liu, Langmuir 26 (2010) 9686.
[44] L.Q. Jing, B.F. Xin, F.L. Yuan, L.P. Xue, B.Q. Wang, H.G. Fu, J. Phys. Chem. B 110 (2006) 17860.